SUPPLEMENTARY DATA

FGF19 Analogue as a Surgical Factor Mimetic That Contributes to Metabolic Effects Beyond Glucose Homeostasis

Alex M. DePaoli, Mei Zhou, Daniel D. Kaplan, Steven C. Hunt, Ted D. Adams, R. Marc Learned, Hui Tian, and Lei Ling*

*Correspondence: Lei Ling, NGM Biopharmaceuticals, Inc., 333 Oyster Point Blvd., South San Francisco, CA 94080; Telephone: 650-243-5546; Email: lling@ngmbio.com

TABLE OF CONTENT

SUPPLEMENTARY DATA

Patients for Gastric Bypass Surgery. Participants were 25 to 60 years of age, with a body mass index (BMI) of 35-60 kg/m^2, had no history of myocardial infarction, coronary bypass surgery, stroke, alcohol or narcotics abuse, had not undergone bariatric surgery, and had not had gastric or duodenal ulcers, a myocardial infarction (in the previous 6 months), or active cancer (in the previous 5 years). The study was reviewed and approved by the institutional review board at the University of Utah in accordance with national guidelines and the provisions of the Helsinki Declaration. All patients provided written informed consent to participate in the study. Patients were evaluated by a multidisciplinary team (including a diabetologist, a dietitian, and a nurse), and serum samples were collected before surgery (baseline) and at 7 and 21 days post surgery.

Animal Experiments. All animal studies were approved by the Institutional Animal Care and Use Committee at NGM.

db/db mice (BKS.Cg-*Dock7*^{m} +/+ *Lepr*^{db}/J, #000642): Beginning at an age of 7 weeks, most *db/db* mice developed severe hyperglycemia (non-fasting blood glucose > 400 mg/dL) accompanied by polyuria, polydipsia, polyphagia. In Figure S1A-D, 11-week old diabetic *db/db* mice received intravenously a total of 1 x 10^{10} genome copies of AAV carrying either FGF19 or a control gene GFP. For the unbiased, *in vivo* screen in *db/db* mice, we designed over 150 FGF19 mutants covering a diverse range of secondary structures (β-sheets, loops, α-helices), and serial deletions at the N- and C-terminus (Table S2-S5, and data not shown). 5 to 6 *db/db* mice were grouped as biological replicates for each FGF19 mutant, providing the coverage necessary to obtain reproducible results, and enabling successful *in vivo* characterization of metabolic and carcinogenic phenotypes. 10-12 week old *db/db* mice were injected intravenously with 3 x 10^{11} vector genome of AAV carrying either FGF19 or a control gene GFP. During the 24-week study periods with continuous exposure to FGF19 mutant transgenes, *db/db* mice were subjected to glucose measurements at various time points, and euthanized at the end of the studies for liver tumor quantification.

TALLYHO mice (TALLYHO/JngJ, #005314): The TALLYHO mouse is an inbred polygenic model for type 2 diabetes showing characteristic signs of hyperglycemia, hyperinsulinemia, hyperleptinemia, but only moderate obesity. 5 week-old TALLYHO mice received a single intravenous injection of 3 x 10^{10} vector genome AAV-FGF19 or AAV-GFP via tail vein. Blood glucose and body weight were measured prior to AAV administration, and at week 3 and 12 after AAV administration. Mice were euthanized at the end of the study for HbA1c measurements.

NONNZO mice (NONcNZO10/LtJ, #004456): The polygenic NONNZO mouse strain typically exhibits hyperglycemia, insulin resistance and obesity. 6 month-old NONNZO mice received a single intravenous injection of 3 x 10^{10} vector genome AAV-FGF19 or AAV-GFP via tail vein. Mice were placed on LabDiet 5K20 diet (Jackson Laboratory) throughout the study. Diets containing metformin (0.2% 1,1-dimethylbiguanide in diet) or pioglitazone (0.05% in diet) were included as positive controls. Blood glucose, body weight, body composition, and HOMA-IR were determined 6 weeks after treatment initiation. For body composition measurements, un-anesthetized mice were placed in “live” probe, and scanned for one minute inside the EcoMRI-5000 whole body composition analyzer. Fat mass was calculated using EcoMRI software from multiple primary accumulation numbers.

STZ mice: C57BL6J mice treated with streptozotocin (STZ) is a non-obese, insulin-deficient mouse model. C57BL/6J (#000664) mice were ***i.p.*** injected daily with 50 mg/kg streptozotocin (Sigma) for 5 days. Blood glucose was monitored every 3 days after the STZ treatment. STZ mice developed severe diabetes with cachexia, and mice with stable, overt diabetes (glucose >400 mg/dL) received a single intravenous injection of 3 x 10^{10} vector genome AAV-FGF19 or AAV-GFP via tail vein. Blood glucose and body weight were measured prior to AAV administration, and at week 4 and 12 after AAV administration. Mice were euthanized at the end of the study for HbA1c, insulin, glucagon measurements.

SUPPLEMENTARY DATA

Transcriptome Profiling, Pathway Analysis and Databases. RNAs were isolated from ileum of Zucker *fa/fa* rats 14 days after DJB or sham surgery, and were treated with DNase I (Thermo Fisher Scientific). RNA integrity and purity were confirmed by Bioanalyzer (Agilent Technologies) with RIN numbers > 9.0. The raw expression data from Affymetrix Rat Gene 1.0 ST whole-transcript arrays were normalized using robust multi-array average (RMA) approach. The metadata and matrix tables have been deposited to the Gene Expression Omnibus (GEO) repository (accession number GSE120530). Ingenuity Pathway Analysis (Qiagen), including canonical pathways, upstream analysis, diseases and functions, was conducted on genes differentially represented in DJB versus sham procedures. Top canonical pathways were ranked by –Log (P value) with threshold P value of 0.05. Highest ranking categories were sorted in a decreasing order of significance.
Microarray datasets (GSE89632, GSE48452 and GSE61260) on patients with non-alcoholic steatohepatitis and normal subjects were extracted from OmicSoft DiseaseLand database (Qiagen), which contains datasets retrieved from a variety of public projects including GEO, SRA (Sequence Read Archive), ArrayExpress, and dbGAP (The Database of Genotypes and Phenotypes). Comparison in gene expression in disease versus normal was conducted using ArrayStudio software version 10.0 from OmicSoft (Qiagen).

Blood parameters. Blood glucose was measured in conscious animals from a hand-held glucometer (Accu-check, Roche Diagnostics) on tail nip blood. Levels of HbA1c were determined on COBAS INTEGRA 400 Plus Clinical Analyzer (Roche Diagnostics) using whole blood. Serum samples were prepared by centrifugation at 4ºC for 10 minutes at 2000g after clotting at room temperature for 30 minutes, for measurements of FGF19 concentrations by enzyme-linked immunosorbent assays (ELISA) (Biovendor, RD191107200R).). Plasma insulin and glucagon were measured with ELISA kits from ALPCO. All assays were performed according to the manufacturers' instructions.

Histology. Tissues were fixed in 10% neutral-buffered formalin and embedded in paraffin. 5 □m sections were deparaffinized in xylenes (5 minutes), rehydrated sequentially in graded ethanol (100%, 95%, 80%, 70%, 50%, 2 minutes each) and PBS (2 minutes). Stains with hematoxylin and eosin, periodic acid-Schiff or Sirius Red were performed using standard process. For osmium tetroxide staining of lipids in the liver, frozen livers were embedded in optimal cutting temperature compound and directly processed for staining. For immunohistochemistry, specimens were subjected to antigen retrieval in a citrate-based Antigen Unmasking Solution (Vector Laboratories, #H-3300), and incubated for 30 minutes with 3% H2O2 at room temperature to block endogenous peroxidase activity. Sections were blocked in PBST (PBS + 0.1% Tween-20) containing 10% goat serum, stained with primary antibodies against insulin (Sigma) or glucagon (Sigma) diluted in blocking solution at 4ºC overnight. Specimens were then washed three times for 5 minutes each in PBST and incubated with biotinylated secondary antibodies in blocking solution for 1 hour at room temperature. Biotinylated secondary antibody, ABC-HRP reagent and DAB colorimetric peroxidase substrate (Vector Laboratories) were used for detection. Digital imaging microscopy was performed using a Leica DM4000 microscope equipped with DFC500 camera (Leica).

DNA constructs. Human FGF19 cDNA (NM005117) was sub-cloned into pAAV-EF1α vector using SpeI and NotI sites with primers 5'- CCGACTAGTCACCATGCGGAGCGGGTGTGTGG -3' (sense) and 5'- ATAAGAATGCGGCCGCTTACTTCTCAAAGCTGGGACTCCTC-3' (antisense). FGF19 mutants were generated by Quick-Change site-directed mutagenesis kit (Agilent Technologies). cDNAs for previously reported FGF19 mutants, FGF2 mutants and chimera were chemically synthesized (DNA2.1).

SUPPLEMENTARY DATA

AAV Production. AAV293 cells (Agilent Technologies) were cultured in Dulbeco's Modification of Eagle's Medium (DMEM; Mediatech) supplemented with 10% fetal bovine serum (FBS) and 1x antibiotic antimycotic solution (Mediatech). Cells were cultured in a humidified incubator with 5% CO2 and 95% air at 37ºC, confirmed to be mycoplasma free, and authenticated by short tandem repeat DNA profiling. The cells were transfected with 3 plasmids (AAV transgene, pHelper (Agilent Technologies) and AAV2/9) for viral production. Viral particles were purified using a discontinued iodixanal (Sigma) gradient and re suspended in phosphate buffered saline (PBS) with 10% glycerol and stored at –80ºC. Viral titer or vector genome number was determined by quantitative PCR using custom Taqman assays specific for Woodchuck hepatitis virus posttranscriptional regulatory element (WPRE) sequences. Standard curves for WPRE were obtained from serial dilutions over a 6 log range of the corresponding plasmids. AAV-mediated gene delivery provides a means to achieve long-lasting transgene expression without the inflammatory responses that are commonly associated with other viral vectors. When introduced into adult mice, sustained expression of up to one year has been observed. The major site of transgene expression is the hepatocytes.

Quantitative PCR with Reverse Transcription (qPCR). Tissues were snap-frozen in liquid nitrogen upon euthanization of animals. Total RNA was extracted using RNeasy Mini kit (Qiagen) and treated with DNase I (Thermo Fisher Scientific). qPCR assays were performed using QuantiTect multiplex qRT-PCR master mix (Qiagen) and premade Taqman gene expression assays (Life Technologies). Samples were loaded into an optical 384-well plate and qPCR were performed in duplicates on QuantStudio 7 Flex Real-Time PCR System (Applied Biosystems). After an initial hold at 50ºC for 30 minutes to allow reverse transcription to complete, HotStart Taq DNA polymerase was activated at 95ºC for 15 minutes. Forty cycles of a three-step PCR (94ºC for 45 seconds, 56ºC for 45 seconds, and 76ºC for 45 seconds) were applied and the fluorescence intensity was measured at each change of temperature to monitor amplification. Target gene expression was determined using the comparative threshold cycle (ΔΔCt) approach and normalized to the expression of housekeeping gene glyceraldehyde 3-phosphate dehydrogenase (GAPDH).

Structural Analysis. The published crystal structures of FGF23-FGFR1-Klotho (PDB code 5W21), FGF19 (PDB code 2P23), and βKlotho (PDB code 5VAQ) were used to build a model of a ternary complex of FGF19-FGFR1-βKlotho using Molecular Operating Environment (MOE) program (Chemical Computing Group). The FGF19-FGFR1-βKlotho 2:2:2 complex was examined for stereo-chemical quality and further optimized via multiple step energy minimizations. Interactions between specific residues in FGF23-FGFR1-Klotho (PDB code 5W21), FGF8-FGFR2 (PDB 2FDB), FGF2-FGFR1-heparin (PDB 1FQ9) were also examined using MOE program. AMBER10:EHT force-field with reaction field implicit solvation was used during analysis.

SUPPLEMENTARY DATA

Supplementary Figure S1. FGF19 Induces Marked, Rapid and Sustained Diabetes Remission in Diabetic Mice.

(A) Study design. Diabetic *db/db* mice, TALLYHO mice, NONNZO mice, or streptozotocin (STZ)-treated mice received a single dose of adeno-associated virus (AAV) carrying FGF19 or green fluorescent protein (GFP) through tail veins. Blood glucose levels were evaluated at various time points.

(B) Blood glucose and body weight over time in *db/db* mice (n=5 mice per group). Note that levels of plasma glucose were significantly reduced from baseline values within 7 days of AAV-FGF19 delivery, and further decreased over time, with no changes in body weight observed, in *db/db* mice

(C) Glycated hemoglobin (HbA1c) and FGF19 levels at the end of the study (12 weeks after AAV administration) in *db/db* mice (n=5 mice per group). Long-term glycemic control was observed with FGF19 treatment, as evidenced by reductions in glycated hemoglobin (HbA1c) levels. Circulating FGF19 levels were 21.5±2.9 ng/mL at the end of the study in these *db/db* mice.

(D) Representative images of pancreatic islets in *db/db* mice. Pancreata were stained with anti-insulin or anti-glucagon antibodies, and developed using DAB substrates (brown color). Slides were counterstained with hematoxylin. n=5 mice per group. FGF19 administration improved β-cell mass and α-cell organization.

(E) Blood glucose and body weight over time, as well as HbA1c and FGF19 levels at the end of the study, in the polygenic, diabetic TALLYHO mice (n=5 mice per group). Note that plasma concentrations of glucose were significantly reduced following AAV-FGF19 injection without weight loss. FGF19 treatment significantly lowered HbA1c levels at the end of the study. Circulating FGF19 levels were 9.9±2.7 ng/mL in these mice.

(F) Glucose, body weight, fat mass and index for homeostasis model assessment of insulin resistance (HOMA-IR) in NONNZO mice (n=5 mice per group). Metformin and pioglitazone, drugs approved for treatment of type 2 diabetes, were included for comparison. Note that comparing with FGF19, treatment with metformin or pioglitazone either resulted in modest reductions in glucose levels or excess weight gain, respectively. FGF19 administration was also accompanied by a marked improvement in insulin sensitivity.

(G) Blood glucose and body weight over time, as well as HbA1c levels at the end of the study, in STZ mice (n=5 mice per group). In contrast to AAV-GFP-injected STZ mice that developed severe hyperglycemia, mice treated with FGF19 remained normoglycemic, with significantly reduced HbA1c levels at the end of the study.

(H) Serum concentrations of insulin and glucagon in STZ mice (n=5 mice per group). Note that administration of FGF19 resulted in suppression of diabetic hyperglucagonemia in STZ mice.

(I) Kidney histology and kidney weight in STZ mice. Scale bars, 2 mm. Magnifications of boxed regions show glomerulosclerosis and an increase in Bowman's capsular space, features of nephropathy, in control STZ mice but not in FGF19-treated STZ mice. Representative Periodic acid–Schiff stained kidney sections were shown. n=5 mice per group.

Values are mean ± SEM. ***P < 0.001, **P < 0.01, *P < 0.05 versus GFP, by two-way analysis of variance (ANOVA) with Sidak's multiple comparisons adjusting for multiple testing (glucose and body weight in panels B, E, G), or one-way ANOVA with Dunnett's multiple comparison tests (panel F), or unpaired, two-tailed t-test (HbA1c in panels C, E, G; insulin and glucagon in panel H; kidney weight in panel I).

SUPPLEMENTARY DATA

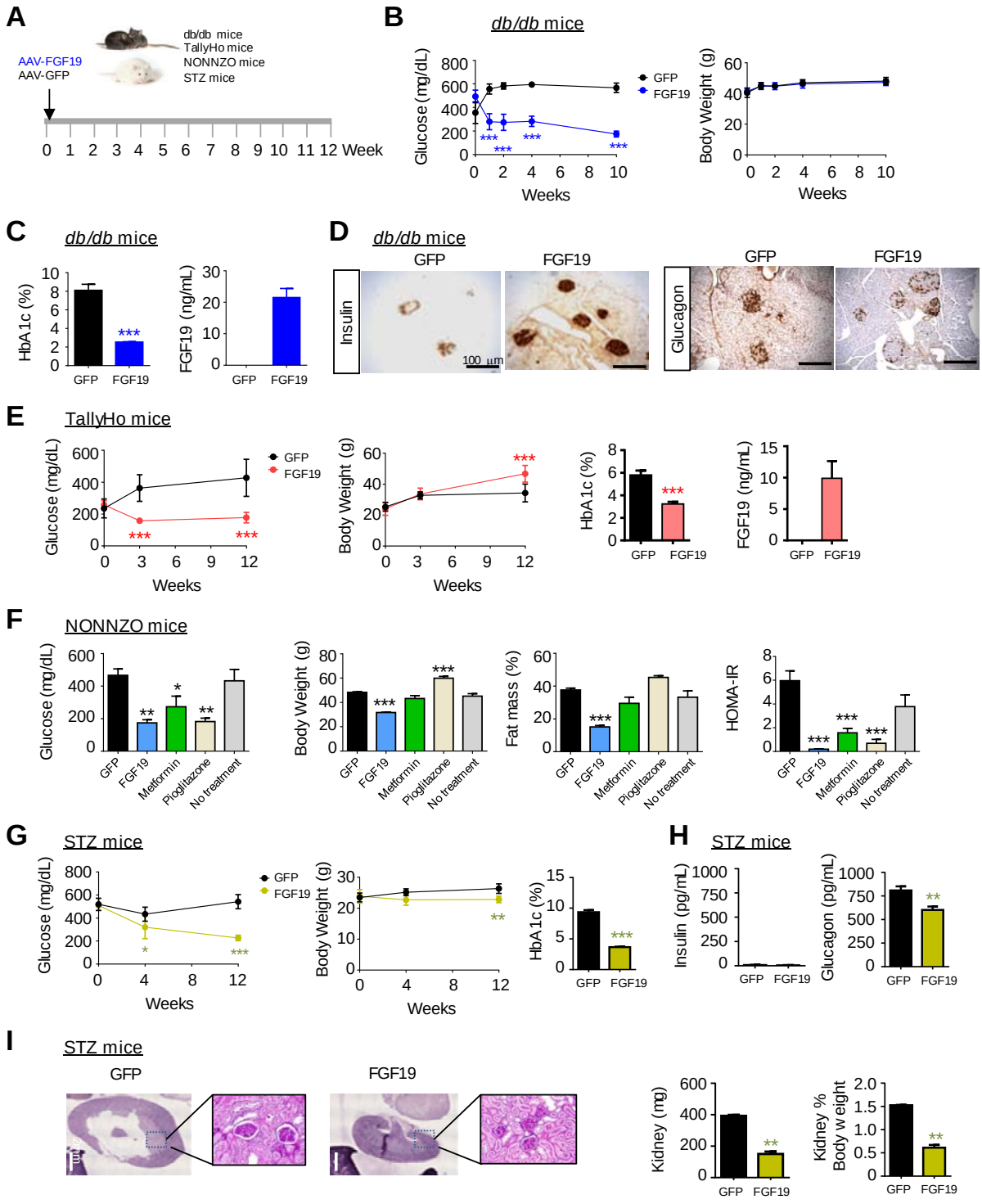

SUPPLEMENTARY DATA

Supplementary Figure S2. Long-Term Evaluation of Previously Reported FGF Mutants in *db/db* Mice.

(A) Glucose results of FGF mutants previously reported (Goetz et al., 2012; Suh et al., 2014; Wu et al., 2011a; Wu et al., 2010). 10-12 week old *db/db* mice were injected intravenously with 3 x 10^{11} vector genome AAV carrying FGF19, FGF mutants, or a control gene GFP. Glucose and body weight were measured before AAV injection (week 0), and at weeks 1, 4, and 24 post AAV injection. n=5-6 mice per group. Although the FGF mutants described in these reports exerted modest glucose-lowering in diet-induced obese mice, possibly secondary to weight reduction in this model, they failed to improve the severe hyperglycemic condition when tested in *db/db* mice. Note that *db/db* mice injected with the FGF2 mutants did not reach the 24-week time point due to reduced survival. n=5-6 mice per group.

(B) Body weights in *db/db* mice expressing FGF mutants previously reported. n=5-6 mice per group.

(C) Liver tumors in *db/db* mice expressing FGF mutants previously reported. *db/db* mice were euthanized at the end of the study (24 weeks after AAV injection) for liver tumor quantification. n=5-6 mice per group.

(D) Liver weight of *db/db* mice expressing FGF mutants previously reported. n=5-6 mice per group.

(E) Kaplan-Meier survival curve. Significant safety concerns (*i.e.*, reduced survival) on these engineered FGF molecules, previously unrecognized from limited cell-based assays, were uncovered upon prolonged exposure in the *db/db* mouse model.

Values are mean ± SEM. ***P < 0.001 by two-way ANOVA with Sidak's multiple comparison tests versus GFP.

SUPPLEMENTARY DATA

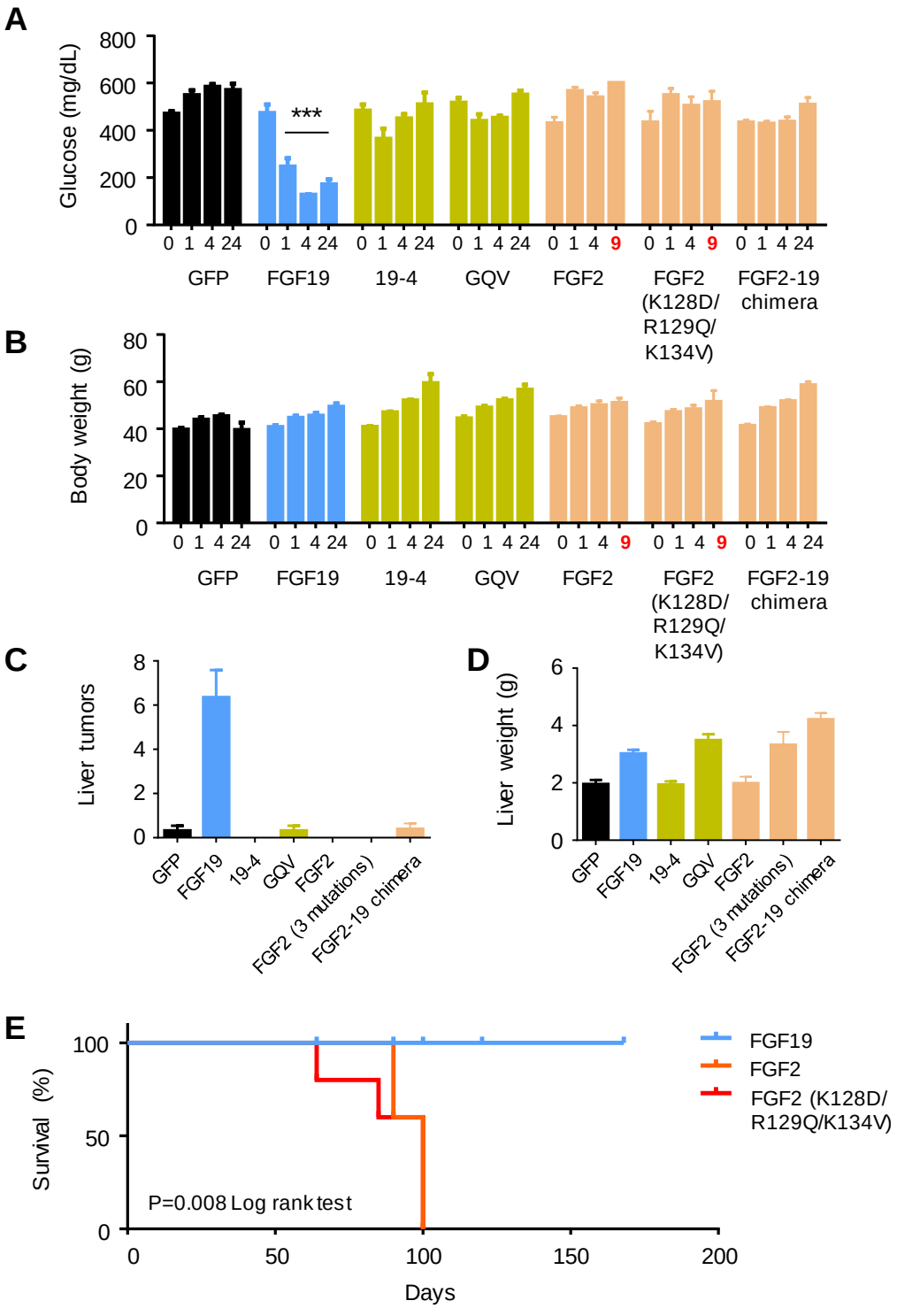

SUPPLEMENTARY DATA

Supplementary Figure S3. *In vivo* Structure-Activity Relationship Analysis of FGF19.

(A) Crystal structure of FGF19 used for mutant design. Shown is PDB 2P23, with β-sheets in FGF19 represented as yellow ribbons, the loops between β-sheets in blue, and the α-helices in red.

(B) Amino acid sequence of FGF19. β-sheets in FGF19 are indicated with yellow ribbons above amino acid sequence, the loops between β-sheets in blue, and the α-helices in red.

(C) Alignment of amino acid sequences in the β8- β9 region. Note that Asp-125 in FGF23 is colored in orange. The β-sheets β8 and β9 are shaded in blue.

(D) A two-dimensional view of interaction between Asp-125 in loop β8-β9 of FGF23 and the invariant Arg-250 in FGFR. An ionic interaction energy of −24.230 kJ/mol was calculated in the FGF23-FGFR1-Klotho structure (PDB 5W21).

(E) Alignment of amino acid sequences in the N-terminal region. Note that key residues directly interact with FGFR in FGF23 (Tyr-25, Pro-26, Asn-27) and FGF8 (Phe-32, His-35, Asp-44, Arg-48) are colored in orange. The changes in the non-tumorigenic FGF19 mutant N1-15 (also known as NGM282 or M70) are colored in blue.

(F) Detailed view of interaction between N-terminus of FGF23 and the D3 domain of FGFR. Left panel, Tyr-25 in FGF23 (yellow ribbon) interacts with Leu-261 and Met-276 in FGFR1 (blue ribbon). Right panel, Pro-26 and Asn-27 in FGF23 interact with Lys-278 in FGFR1.

(G) Detailed view of interaction between N-terminus of FGF8 and the D3 domain of FGFR. Arg-48 in FGF8 (yellow ribbon) interacts with Glu-2325 in FGFR2 (blue ribbon), with an ionic interaction energy of −26.574 kJ/mol; Asp-44 in FGF8 interacts with His-2387 in FGFR2, with a hydrogen bond energy of −5.993 kJ/mol; His-35 in FGF8 interacts with Gln-2389 in FGFR2, with a hydrogen bond energy of −5.865 kJ/mol; Phe-32 in FGF8 forms van der Waals (VdW) interactions with multiple residues in FGFR2.

Values are mean ± SEM. ***P < 0.001 by two-way ANOVA with Sidak's multiple comparison tests versus GFP.

SUPPLEMENTARY DATA

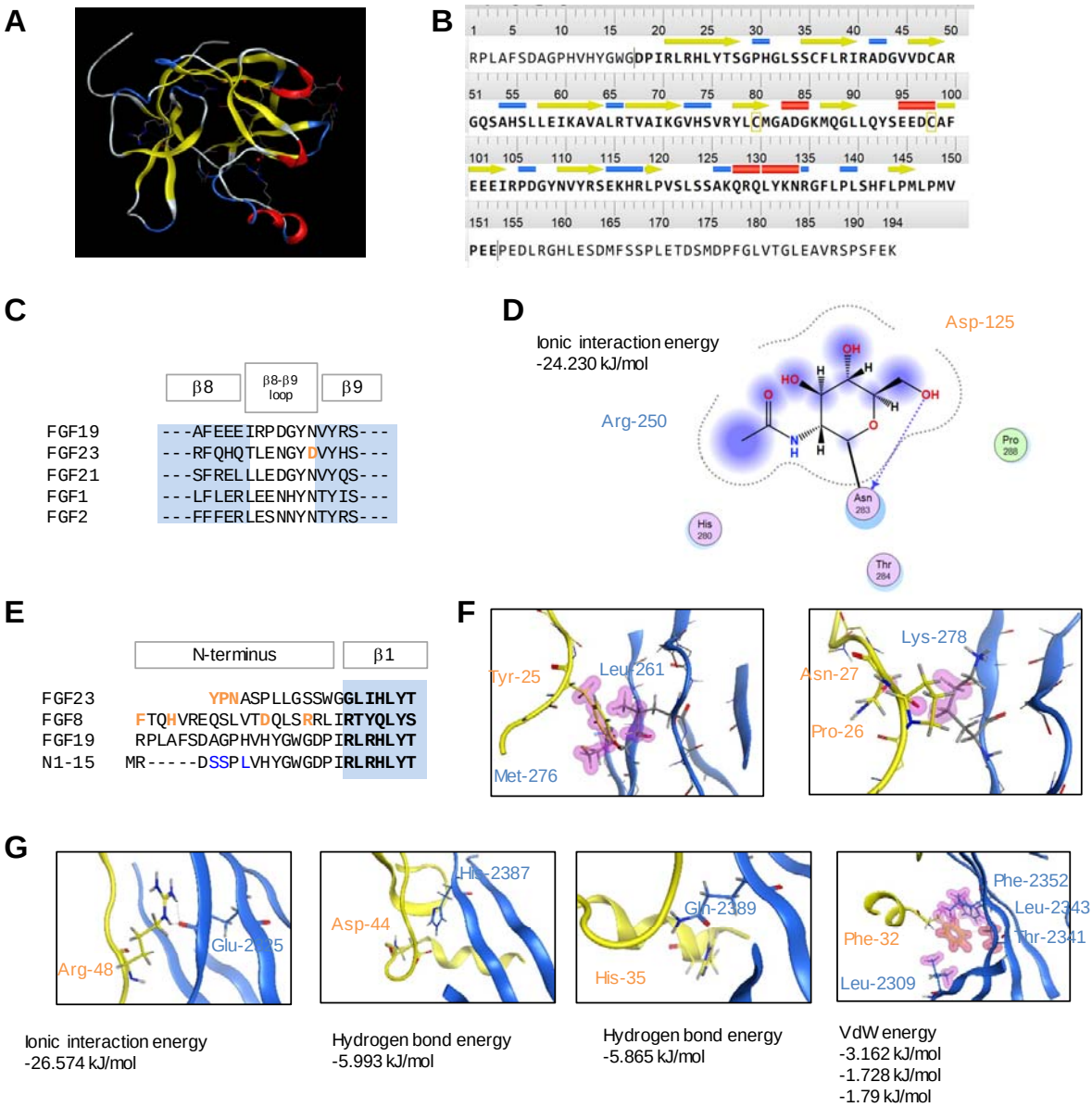

SUPPLEMENTARY DATA

Supplementary Figure S4. *In vivo* Structure-Activity Relationship Analysis of FGF19 in the C-terminal Region.

(A) Alignment of amino acid sequences in the C-terminal region. Note that Asp-212 in FGF19 is colored in red, and Arg-187 in FGF23 is colored in orange. The β-sheet β11 is shaded in blue. Molecular modeling of the FGF19- βKlotho-FGFR1 complex positions the C-terminus of FGF19 to insert into the KL1-KL2 cleft of βKlotho and further dip into the central barrel of KL2, similar to the FGF23-Klotho and FGF21- βKlotho interactions. By gripping the outreaching C-terminal tail, βKlotho anchors the FGF19-FGFR complex.

(B) Interaction between FGF19 C-tail and βKlotho. Left panel, energy of interactions in ascending order; right panel, detailed view of ionic interaction between Asp-212 in FGF19 (red) and Lys-387 in βKlotho (green). Modeling also suggests that FGF19 C-tail forms stronger interaction with βKlotho than FGF21, or contacts between FGF23C and Klotho. This increase in affinity is mainly attributable to the unique Asp-212 residue in FGF19 that forms ionic interaction with Lys-387 of βKlotho.

(C) Interaction between FGF23 C-tail and Klotho. Left panel, energy of interactions in ascending order; right panel, detailed view of contacts between Arg-187 in FGF23 (yellow) and multiple residues in Klotho (green).

(D) Interaction between FGF21 C-tail and βKlotho. Left panel, energy of interactions in ascending order; note that the interaction between FGF21C and βKlotho is weaker than FGF19C-βKlotho or FGF23C-Klotho. Right panel, lack of contact between Leu-194 in FGF21 (grey) and βKlotho (green).

(E) *in vivo* screen of FGF19 mutants with deletions in the C-terminal region. 10-12 week old *db/db* mice were injected intravenously with 3×10^{11} vector genome AAV carrying FGF19, FGF19 mutants, or a control gene GFP. Blood glucose was measured before AAV injection (week 0), and at weeks 4 and 24 post AAV injection. Mice were euthanized at the end of the study (24 weeks after AAV injection) for liver tumor and liver weight quantification. n=5-6 mice per group. Consistent with the molecular interactions depicted in panel B, deletion of 30 amino acids from the C-terminus completely abolished FGF19's ability to lower glucose in *db/db* mice.

Values are mean ± SEM. ***P < 0.001 by two-way ANOVA with Sidak's multiple comparison tests versus GFP.

SUPPLEMENTARY DATA

A

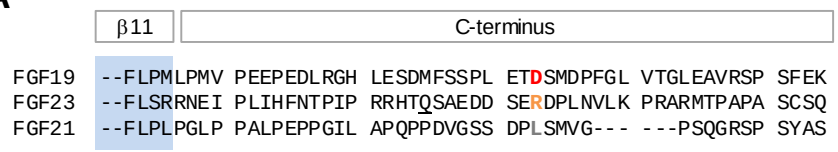

B

FGF19 C-terminus

Type	ChainA	PosA	SetA	ChainB	PosB	SetB	Energy ▲
DIH	1-F19	156	Asp212	2-KLB	323	Lys387	-27.735
DIH	1-F19	177	Lys233	2-KLB	601	Arg703	-18.210
DH	1-F19	168	Glu224	2-KLB	746	Gln848	-10.346
DIH	1-F19	168	Glu224	2-KLB	743	Arg845	-8.952
DH	1-F19	172	Ser228	2-KLB	740	Asp842	-7.718
DH	1-F19	177	Lys233	2-KLB	600	Asn702	-6.036
DH	1-F19	168	Glu224	2-KLB	747	Phe849	-5.870
DH	1-F19	174	Ser230	2-KLB	738	Arg840	-5.703

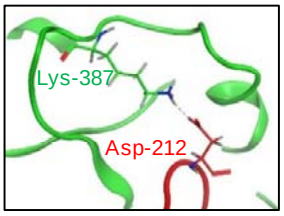

C

FGF23 C-terminus

Type	ChainA	PosA	SetA	ChainB	PosB	SetB	Energy ▲
DIH	2-F23	220	Arg198	1-KL	756	Asp756	-12.038
DI	2-F23	209	Arg187	1-KL	820	Asp820	-10.312
DH	2-F23	218	Arg196	1-KL	832	Glu832	-4.978
DIH	2-F23	206	Asp184	1-KL	385	Lys385	-4.788
DH	2-F23	214	Val192	1-KL	834	Thr834	-4.111
DIH	2-F23	218	Arg196	1-KL	756	Asp756	-4.016

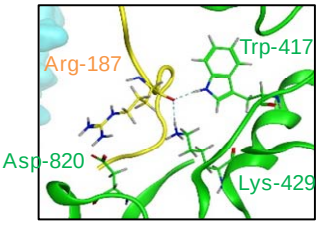

D

FGF21 C-terminus

Type	ChainA	PosA	SetA	ChainB	PosB	SetB	Energy ▲
DH	2-F21	16	Gln201	1-KLB	816	Arg845	-5.418
DH	2-F21	13	Gly198	1-KLB	820	Phe849	-5.125
DH	2-F21	21	Ser206	1-KLB	664	Glu693	-3.887
DH	2-F21	22	Tyr207	1-KLB	617	His646	-3.758
DH	2-F21	6	Ser191	1-KLB	393	Asp422	-3.709
DH	2-F21	11	Met196	1-KLB	822	Gln851	-3.641

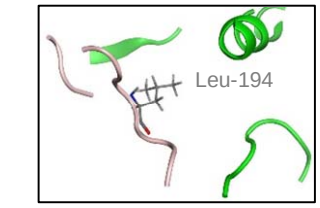

E

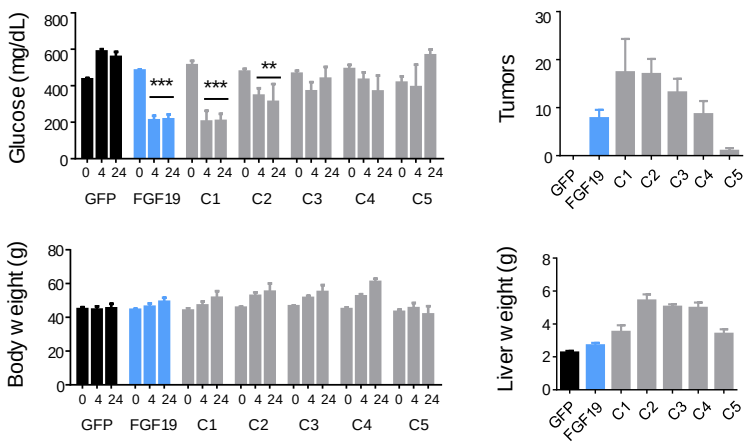

SUPPLEMENTARY DATA

Supplementary Figure S5. *In vivo* Structure-Activity Relationship Analysis of FGF19 in the Heparin-Binding Region.

(A) Molecular model of FGF19-FGFR1-heparin 2:2:2 ternary complex. Crystal structure of FGF19 (PDB 2P23) was superimposed onto the FGF2-FGFR1-heparin complex (PDB 1FQ9). FGF19 and FGFR1 are shown in the surface representation in red and blue, respectively; heparin is shown in yellow sticks. The model is rotated 90º between the left and right panels.

(B) Expanded view of interaction site between FGF19 and heparin. Key FGF19 residues that are in contact with heparin are labeled in cyan.

(C) Glucose results from *in vivo* screen of FGF19 mutants in heparin-binding region. 10-12 week old *db/db* mice were injected intravenously with 3 x 10^{11} vector genome AAV carrying FGF19, FGF19 mutants, or a control gene GFP. Glucose and body weight were measured before AAV injection (week 0), and at weeks 1, 5 and 14 post AAV injection. In summary, we found that FGF19 mutants containing single amino acid substitutions (i.e. Lys-149, Arg-151, Lys-155, or Arg-157) retained anti-diabetic activity, while the combination of these mutations compromised the glucoregulatory activity of the corresponding FGF19 variants.

(D) Body weights of *db/db* mice expressing FGF19 mutants in heparin-binding region.

(E) Liver tumors in *db/db* mice expressing FGF19 mutants in heparin-binding region. *db/db* mice were euthanized at the end of the study (24 weeks after AAV injection) for liver tumor quantification. Notably, evidence for hepatic tumorigenesis was clearly observed in *db/db* mice expressing FGF19 with mutations in heparin-binding region. Collectively, these studies suggest that the residual heparin binding exhibited by FGF19 does not appear to play a significant role in FGF19-associated hepatocarcinogenesis.

(F) Liver weight of *db/db* mice expressing FGF19 mutants in heparin-binding region.

Values are mean ± SEM. ***P < 0.001 by two-way ANOVA with Sidak's multiple comparison tests versus GFP.

SUPPLEMENTARY DATA

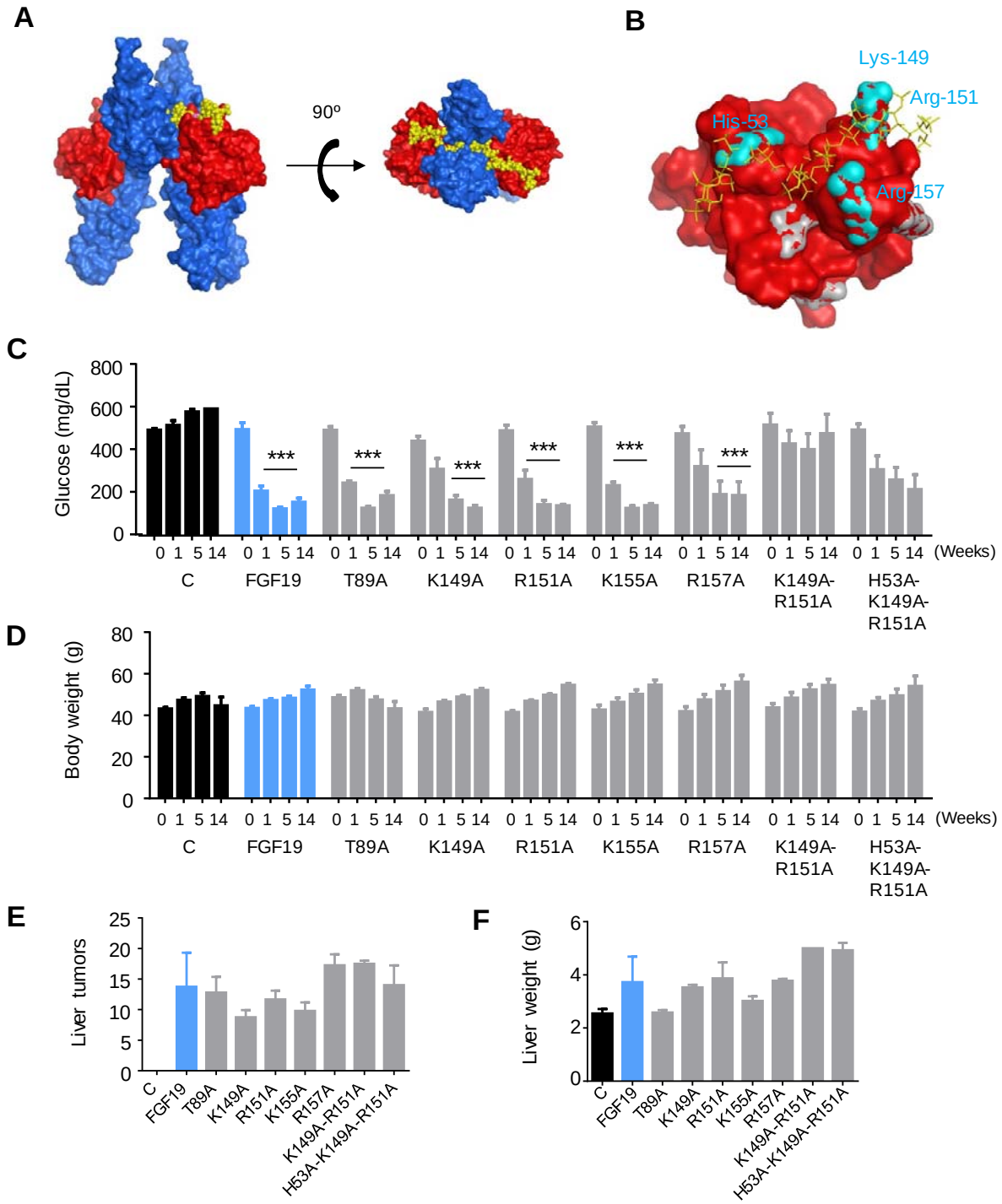

SUPPLEMENTARY DATA

Supplementary Table S1. Gastric Bypass Subject Characteristics at Baseline, and at Day 7 and Day 21 Post Surgery (N=29)

Variable	Baseline	Day 7	Day 21
Sex (female%)	69%	---	---
Age (year)	47.5±8.5	---	---
Fasting glucose (mg/dL)	113±43	112±40	100±36
HbA1c (%)	7.1±1.2	6.7±1.0***	6.3±0.8***
Total cholesterol (mg/dL)	167±40	173±32	145±35**
HDL-C (mg/dL)	42.0±10.3	33.8±6.3***	34.8±6.9***
LDL-C (mg/dL)	110±34	123±30*	98±33
Triglycerides (mg/dL)	167±53	169±64	139±54*
Weight (kg)	130±29	125±28***	119±27***
Height (cm)	167±9	---	---
BMI (kg/m^2)	46.2±9.8	44.2±9.7***	42.4±9.8***
Waist circumference (cm)	135±18	129±19***	127±19***
Body Fat (%)	48.8±12.4	---	45.9±12.1***
SBP (mm Hg)	122±15	120±16	113±18**
DBP (mm Hg)	72±8	69±9	67±8**
Treated hypertension, %	52%	---	---
Treated dyslipidemia, %	59%	---	---
Diabetes duration (year)	5.7±5.4	---	---

BMI, body mass index; DBP, diastolic blood pressure; HDL-C, high-density lipoprotein cholesterol; LDL-C, low-density lipoprotein cholesterol; SBP, systolic blood pressure

SUPPLEMENTARY DATA

Supplementary Table S2. Sequence of FGF19 Mutants in the Loop Regions.

Name	Amino Acid Sequence
FGF19	RPLAFSDAGPHVHYGWGDPIRLRHLYTSGPHGLSSCFLRIRADGVVDCAR GQSAHSLLEIKAVALRTVAIKGVHSVRYLCMGADGKMQGLLQYSEEDCAF EEEIRPDGYNVYRSEKHRLPVSLSSAKQRQLYKNRGFLPLSHFLPMLPMV PEEPEDLRGHLESDMFSSPLETDSMDPFGLVTGLEAVRSPSFEK
β1- β2	RPLAFSDAGPHVHYGWGDPIRLRHLYTDDAQ-QTSCFLRIRADGVVDCAR GQSAHSLLEIKAVALRTVAIKGVHSVRYLCMGADGKMQGLLQYSEEDCAF EEEIRPDGYNVYRSEKHRLPVSLSSAKQRQLYKNRGFLPLSHFLPMLPMV PEEPEDLRGHLESDMFSSPLETDSMDPFGLVTGLEAVRSPSFEK
β2- β3	RPLAFSDAGPHVHYGWGDPIRLRHLYTSGPHGLSSCFLRIREDGVVDCAR GQSAHSLLEIKAVALRTVAIKGVHSVRYLCMGADGKMQGLLQYSEEDCAF EEEIRPDGYNVYRSEKHRLPVSLSSAKQRQLYKNRGFLPLSHFLPMLPMV PEEPEDLRGHLESDMFSSPLETDSMDPFGLVTGLEAVRSPSFEK
β3- β4	RPLAFSDAGPHVHYGWGDPIRLRHLYTSGPHGLSSCFLRIRADGVVDCAA DQSPHSLLEIKAVALRTVAIKGVHSVRYLCMGADGKMQGLLQYSEEDCAF EEEIRPDGYNVYRSEKHRLPVSLSSAKQRQLYKNRGFLPLSHFLPMLPMV PEEPEDLRGHLESDMFSSPLETDSMDPFGLVTGLEAVRSPSFEK
β4- β5	RPLAFSDAGPHVHYGWGDPIRLRHLYTSGPHGLSSCFLRIRADGVVDCAR GQSAHSLLEIKAVKPGVVAIKGVHSVRYLCMGADGKMQGLLQYSEEDCAF EEEIRPDGYNVYRSEKHRLPVSLSSAKQRQLYKNRGFLPLSHFLPMLPMV PEEPEDLRGHLESDMFSSPLETDSMDPFGLVTGLEAVRSPSFEK
β5- β6	RPLAFSDAGPHVHYGWGDPIRLRHLYTSGPHGLSSCFLRIRADGVVDCAR GQSAHSLLEIKAVALRTVAIKGVKTVRYLCMGADGKMQGLLQYSEEDCAF EEEIRPDGYNVYRSEKHRLPVSLSSAKQRQLYKNRGFLPLSHFLPMLPMV PEEPEDLRGHLESDMFSSPLETDSMDPFGLVTGLEAVRSPSFEK
β6- β7	RPLAFSDAGPHVHYGWGDPIRLRHLYTSGPHGLSSCFLRIRADGVVDCAR GQSAHSLLEIKAVALRTVAIKGVHSVRYLCMGPDGKMQGLLQYSEEDCAF EEEIRPDGYNVYRSEKHRLPVSLSSAKQRQLYKNRGFLPLSHFLPMLPMV PEEPEDLRGHLESDMFSSPLETDSMDPFGLVTGLEAVRSPSFEK
β7- β8	RPLAFSDAGPHVHYGWGDPIRLRHLYTSGPHGLSSCFLRIRADGVVDCAR GQSAHSLLEIKAVALRTVAIKGVHSVRYLCMGADGKMQGSLHFDEEDCAF EEEIRPDGYNVYRSEKHRLPVSLSSAKQRQLYKNRGFLPLSHFLPMLPMV PEEPEDLRGHLESDMFSSPLETDSMDPFGLVTGLEAVRSPSFEK
β8- β9	RPLAFSDAGPHVHYGWGDPIRLRHLYTSGPHGLSSCFLRIRADGVVDCAR GQSAHSLLEIKAVALRTVAIKGVHSVRYLCMGADGKMQGLLQYSEEDCAF EEEILEDGYNVYRSEKHRLPVSLSSAKQRQLYKNRGFLPLSHFLPMLPMV PEEPEDLRGHLESDMFSSPLETDSMDPFGLVTGLEAVRSPSFEK
β9- β10	RPLAFSDAGPHVHYGWGDPIRLRHLYTSGPHGLSSCFLRIRADGVVDCAR GQSAHSLLEIKAVALRTVAIKGVHSVRYLCMGADGKMQGLLQYSEEDCAF EEEIRPDGYNVYRSEAHRLPVSLSSAKQRQLYKNRGFLPLSHFLPMLPMV PEEPEDLRGHLESDMFSSPLETDSMDPFGLVTGLEAVRSPSFEK
β10- αH	RPLAFSDAGPHVHYGWGDPIRLRHLYTSGPHGLSSCFLRIRADGVVDCAR GQSAHSLLEIKAVALRTVAIKGVHSVRYLCMGADGKMQGLLQYSEEDCAF EEEIRPDGYNVYRSEKHRLPLHLPGNKQRQLYKNRGFLPLSHFLPMLPMV PEEPEDLRGHLESDMFSSPLETDSMDPFGLVTGLEAVRSPSFEK
αH- β11	RPLAFSDAGPHVHYGWGDPIRLRHLYTSGPHGLSSCFLRIRADGVVDCAR GQSAHSLLEIKAVALRTVAIKGVHSVRYLCMGADGKMQGLLQYSEEDCAF

SUPPLEMENTARY DATA

	EEEIRPDGYNVYRSEKHRLPVSLSSAKQRQLYKNRGPARFLPLSHFLPML PMVPEEPEDLRGHLESDMFSSPLETDSMDPFGLVTGLEAVRSPSFEK

Amino acids that differ from wild type FGF19 are shown in red. β1- β2 indicates mutations in the loop region between β-sheets β1 and β2; β10- αH indicates mutations in the loop region between β-sheet β10 and the α-helix located immediately after β10.

SUPPLEMENTARY DATA

Supplementary Table S3. Sequence of FGF19 Mutants in the β-Sheet Regions

Name	Amino Acid Sequence
FGF19	RPLAFSDAGPHVHYGWGDPIRLRHLYTSGPHGLSSCFLRIRADGVVDCAR GQSAHSLLEIKAVALRTVAIKGVHSVRYLCMGADGKMQGLLQYSEEDCAF EEEIRPDGYNVYRSEKHRLPVSLSSAKQRQLYKNRGFLPLSHFLPMLPMV PEEPEDLRGHLESDMFSSPLETDSMDPFGLVTGLEAVRSPSFEK
β1	RPLAFSDAGPHVHYGWGDPIRQRHLYTSGPHGLSSCFLRIRADGVVDCAR GQSAHSLLEIKAVALRTVAIKGVHSVRYLCMGADGKMQGLLQYSEEDCAF EEEIRPDGYNVYRSEKHRLPVSLSSAKQRQLYKNRGFLPLSHFLPMLPMV PEEPEDLRGHLESDMFSSPLETDSMDPFGLVTGLEAVRSPSFEK
β2	RPLAFSDAGPHVHYGWGDPIRLRHLYTSGPHGLSEAHLEIRADGVVDCAR GQSAHSLLEIKAVALRTVAIKGVHSVRYLCMGADGKMQGLLQYSEEDCAF EEEIRPDGYNVYRSEKHRLPVSLSSAKQRQLYKNRGFLPLSHFLPMLPMV PEEPEDLRGHLESDMFSSPLETDSMDPFGLVTGLEAVRSPSFEK
β3	RPLAFSDAGPHVHYGWGDPIRLRHLYTSGPHGLSSCFLRIRADGTVGGAR GQSAHSLLEIKAVALRTVAIKGVHSVRYLCMGADGKMQGLLQYSEEDCAF EEEIRPDGYNVYRSEKHRLPVSLSSAKQRQLYKNRGFLPLSHFLPMLPMV PEEPEDLRGHLESDMFSSPLETDSMDPFGLVTGLEAVRSPSFEK
β4	RPLAFSDAGPHVHYGWGDPIRLRHLYTSGPHGLSSCFLRIRADGVVDCAR GQSAESLLQLKALALRTVAIKGVHSVRYLCMGADGKMQGLLQYSEEDCAF EEEIRPDGYNVYRSEKHRLPVSLSSAKQRQLYKNRGFLPLSHFLPMLPMV PEEPEDLRGHLESDMFSSPLETDSMDPFGLVTGLEAVRSPSFEK
β5	RPLAFSDAGPHVHYGWGDPIRLRHLYTSGPHGLSSCFLRIRADGVVDCAR GQSAHSLLEIKAVALRTIQILGVHSVRYLCMGADGKMQGLLQYSEEDCAF EEEIRPDGYNVYRSEKHRLPVSLSSAKQRQLYKNRGFLPLSHFLPMLPMV PEEPEDLRGHLESDMFSSPLETDSMDPFGLVTGLEAVRSPSFEK
β6	RPLAFSDAGPHVHYGWGDPIRLRHLYTSGPHGLSSCFLRIRADGVVDCAR GQSAHSLLEIKAVALRTVAIKGVHSSRFLCQRADGKMQGLLQYSEEDCAF EEEIRPDGYNVYRSEKHRLPVSLSSAKQRQLYKNRGFLPLSHFLPMLPMV PEEPEDLRGHLESDMFSSPLETDSMDPFGLVTGLEAVRSPSFEK
β7	RPLAFSDAGPHVHYGWGDPIRLRHLYTSGPHGLSSCFLRIRADGVVDCAR GQSAHSLLEIKAVALRTVAIKGVHSVRYLCMGADGALYGLLQYSEEDCAF EEEIRPDGYNVYRSEKHRLPVSLSSAKQRQLYKNRGFLPLSHFLPMLPMV PEEPEDLRGHLESDMFSSPLETDSMDPFGLVTGLEAVRSPSFEK
β8	RPLAFSDAGPHVHYGWGDPIRLRHLYTSGPHGLSSCFLRIRADGVVDCAR GQSAHSLLEIKAVALRTVAIKGVHSVRYLCMGADGKMQGLLQYSPEACSF RELLRPDGYNVYRSEKHRLPVSLSSAKQRQLYKNRGFLPLSHFLPMLPMV PEEPEDLRGHLESDMFSSPLETDSMDPFGLVTGLEAVRSPSFEK
β9	RPLAFSDAGPHVHYGWGDPIRLRHLYTSGPHGLSSCFLRIRADGVVDCAR GQSAHSLLEIKAVALRTVAIKGVHSVRYLCMGADGKMQGLLQYSEEDCAF EEEIRPDGYNVYQSEKHRLPVSLSSAKQRQLYKNRGFLPLSHFLPMLPMV PEEPEDLRGHLESDMFSSPLETDSMDPFGLVTGLEAVRSPSFEK
β10	RPLAFSDAGPHVHYGWGDPIRLRHLYTSGPHGLSSCFLRIRADGVVDCAR GQSAHSLLEIKAVALRTVAIKGVHSVRYLCMGADGKMQGLLQYSEEDCAF EEEIRPDGYNVYRSEKHGLPLHLPGAKQRQLYKNRGFLPLSHFLPMLPMV PEEPEDLRGHLESDMFSSPLETDSMDPFGLVTGLEAVRSPSFEK
β11	RPLAFSDAGPHVHYGWGDPIRLRHLYTSGPHGLSSCFLRIRADGVVDCAR

SUPPLEMENTARY DATA

	GQSAHSLLEIKAVALRTVAIKGVHSVRYLCMGADGKMQGLLQYSEEDCAF EEEIRPDGYNVYRSEKHRLPVSLSSAKQRQLYKNRGFLPLSHLPPALPMV PEEPEDLRGHLESDMFSSPLETDSMDPFGLVTGLEAVRSPSFEK
αH	RPLAFSDAGPHVHYGWGDPIRLRHLYTSGPHGLSSCFLRIRADGVVDCAR GQSAHSLLEIKAVALRTVAIKGVHSVRYLCMGADGKMQGLLQYSEEDCAF EEEIRPDGYNVYRSEKHRLPVSLSSNKSPHRDPAPRGFLPLSHFLPMLPMV PEEPEDLRGHLESDMFSSPLETDSMDPFGLVTGLEAVRSPSFEK

Amino acids that differ from wild type FGF19 are shown in red. β1 indicates mutations in β-sheet 1. αH indicates mutations in the α-helix located immediately after β10. None of the FGF19 mutants in the β-sheet region were non-tumorigenic while retaining the anti-diabetic effects (data not shown).

SUPPLEMENTARY DATA

Supplementary Table S4. Sequence of FGF19 Mutants in the N-terminal Region

Name	Amino Acid Sequence
FGF19	RPLAFSDAGPHVHYGWGDPIRLRHLYTSGPHGLSSCFLRIRADGVVDCAR GQSAHSLLEIKAVALRTVAIKGVHSVRYLCMGADGKMQGLLQYSEEDCAF EEEIRPDGYNVYRSEKHRLPVSLSSAKQRQLYKNRGFLPLSHFLPMLPMV PEEPEDLRGHLESDMFSSPLETDSMDPFGLVTGLEAVRSPSFEK
N1	R-----DAGPHVHYGWGDPIRLRHLYTSGPHGLSSCFLRIRADGVVDCAR GQSAHSLLEIKAVALRTVAIKGVHSVRYLCMGADGKMQGLLQYSEEDCAF EEEIRPDGYNVYRSEKHRLPVSLSSAKQRQLYKNRGFLPLSHFLPMLPMV PEEPEDLRGHLESDMFSSPLETDSMDPFGLVTGLEAVRSPSFEK
N2	R----------VHYGWGDPIRLRHLYTSGPHGLSSCFLRIRADGVVDCAR GQSAHSLLEIKAVALRTVAIKGVHSVRYLCMGADGKMQGLLQYSEEDCAF EEEIRPDGYNVYRSEKHRLPVSLSSAKQRQLYKNRGFLPLSHFLPMLPMV PEEPEDLRGHLESDMFSSPLETDSMDPFGLVTGLEAVRSPSFEK
N3	R---------------GDPIRLRHLYTSGPHGLSSCFLRIRADGVVDCAR GQSAHSLLEIKAVALRTVAIKGVHSVRYLCMGADGKMQGLLQYSEEDCAF EEEIRPDGYNVYRSEKHRLPVSLSSAKQRQLYKNRGFLPLSHFLPMLPMV PEEPEDLRGHLESDMFSSPLETDSMDPFGLVTGLEAVRSPSFEK
N1-1	R-----DEDPLVHYGWGDPIRLRHLYTSGPHGLSSCFLRIRADGVVDCAR GQSAHSLLEIKAVALRTVAIKGVHSVRYLCMGADGKMQGLLQYSEEDCAF EEEIRPDGYNVYRSEKHRLPVSLSSAKQRQLYKNRGFLPLSHFLPMLPMV PEEPEDLRGHLESDMFSSPLETDSMDPFGLVTGLEAVRSPSFEK
N1-2	R-----DEGPLVHYGWGDPIRLRHLYTSGPHGLSSCFLRIRADGVVDCAR GQSAHSLLEIKAVALRTVAIKGVHSVRYLCMGADGKMQGLLQYSEEDCAF EEEIRPDGYNVYRSEKHRLPVSLSSAKQRQLYKNRGFLPLSHFLPMLPMV PEEPEDLRGHLESDMFSSPLETDSMDPFGLVTGLEAVRSPSFEK
N1-3	R-----DEDPHVHYGWGDPIRLRHLYTSGPHGLSSCFLRIRADGVVDCAR GQSAHSLLEIKAVALRTVAIKGVHSVRYLCMGADGKMQGLLQYSEEDCAF EEEIRPDGYNVYRSEKHRLPVSLSSAKQRQLYKNRGFLPLSHFLPMLPMV PEEPEDLRGHLESDMFSSPLETDSMDPFGLVTGLEAVRSPSFEK
N1-4	R-----DEGPHVHYGWGDPIRLRHLYTSGPHGLSSCFLRIRADGVVDCAR GQSAHSLLEIKAVALRTVAIKGVHSVRYLCMGADGKMQGLLQYSEEDCAF EEEIRPDGYNVYRSEKHRLPVSLSSAKQRQLYKNRGFLPLSHFLPMLPMV PEEPEDLRGHLESDMFSSPLETDSMDPFGLVTGLEAVRSPSFEK
N1-5	R-----DQGPHVHYGWGDPIRLRHLYTSGPHGLSSCFLRIRADGVVDCAR GQSAHSLLEIKAVALRTVAIKGVHSVRYLCMGADGKMQGLLQYSEEDCAF EEEIRPDGYNVYRSEKHRLPVSLSSAKQRQLYKNRGFLPLSHFLPMLPMV PEEPEDLRGHLESDMFSSPLETDSMDPFGLVTGLEAVRSPSFEK
N1-6	R-----DQGLHVHYGWGDPIRLRHLYTSGPHGLSSCFLRIRADGVVDCAR GQSAHSLLEIKAVALRTVAIKGVHSVRYLCMGADGKMQGLLQYSEEDCAF EEEIRPDGYNVYRSEKHRLPVSLSSAKQRQLYKNRGFLPLSHFLPMLPMV PEEPEDLRGHLESDMFSSPLETDSMDPFGLVTGLEAVRSPSFEK
N1-7	R-----DQSPHVHYGWGDPIRLRHLYTSGPHGLSSCFLRIRADGVVDCAR GQSAHSLLEIKAVALRTVAIKGVHSVRYLCMGADGKMQGLLQYSEEDCAF EEEIRPDGYNVYRSEKHRLPVSLSSAKQRQLYKNRGFLPLSHFLPMLPMV PEEPEDLRGHLESDMFSSPLETDSMDPFGLVTGLEAVRSPSFEK
N1-8	R-----DESPHVHYGWGDPIRLRHLYTSGPHGLSSCFLRIRADGVVDCAR GQSAHSLLEIKAVALRTVAIKGVHSVRYLCMGADGKMQGLLQYSEEDCAF

SUPPLEMENTARY DATA

	EEEIRPDGYNVYRSEKHRLPVSLSSAKQRQLYKNRGFLPLSHFLPMLPMV PEEPEDLRGHLESDMFSSPLETDSMDPFGLVTGLEAVRSPSFEK
N1-9	R-----DQSPLVHYGWGDPIRLRHLYTSGPHGLSSCFLRIRADGVVDCAR GQSAHSLLEIKAVALRTVAIKGVHSVRYLCMGADGKMQGLLQYSEEDCAF EEEIRPDGYNVYRSEKHRLPVSLSSAKQRQLYKNRGFLPLSHFLPMLPMV PEEPEDLRGHLESDMFSSPLETDSMDPFGLVTGLEAVRSPSFEK
N1-10	R-----DESPLVHYGWGDPIRLRHLYTSGPHGLSSCFLRIRADGVVDCAR GQSAHSLLEIKAVALRTVAIKGVHSVRYLCMGADGKMQGLLQYSEEDCAF EEEIRPDGYNVYRSEKHRLPVSLSSAKQRQLYKNRGFLPLSHFLPMLPMV PEEPEDLRGHLESDMFSSPLETDSMDPFGLVTGLEAVRSPSFEK
N1-11	R-----DASPLVHYGWGDPIRLRHLYTSGPHGLSSCFLRIRADGVVDCAR GQSAHSLLEIKAVALRTVAIKGVHSVRYLCMGADGKMQGLLQYSEEDCAF EEEIRPDGYNVYRSEKHRLPVSLSSAKQRQLYKNRGFLPLSHFLPMLPMV PEEPEDLRGHLESDMFSSPLETDSMDPFGLVTGLEAVRSPSFEK
N1-12	R-----DSSPHVHYGWGDPIRLRHLYTSGPHGLSSCFLRIRADGVVDCAR GQSAHSLLEIKAVALRTVAIKGVHSVRYLCMGADGKMQGLLQYSEEDCAF EEEIRPDGYNVYRSEKHRLPVSLSSAKQRQLYKNRGFLPLSHFLPMLPMV PEEPEDLRGHLESDMFSSPLETDSMDPFGLVTGLEAVRSPSFEK
N1-13	R-----DSGPLVHYGWGDPIRLRHLYTSGPHGLSSCFLRIRADGVVDCAR GQSAHSLLEIKAVALRTVAIKGVHSVRYLCMGADGKMQGLLQYSEEDCAF EEEIRPDGYNVYRSEKHRLPVSLSSAKQRQLYKNRGFLPLSHFLPMLPMV PEEPEDLRGHLESDMFSSPLETDSMDPFGLVTGLEAVRSPSFEK
N1-14	R-----DSSPLVHYGWGDPIRLRHLYTSGPHGLSSCFLRIRADGVVDCAR GQSAHSLLEIKAVALRTVAIKGVHSVRYLCMGADGKMQGLLQYSEEDCAF EEEIRPDGYNVYRSEKHRLPVSLSSAKQRQLYKNRGFLPLSHFLPMLPMV PEEPEDLRGHLESDMFSSPLETDSMDPFGLVTGLEAVRSPSFEK
N1-15	MR----DSSPLVHYGWGDPIRLRHLYTSGPHGLSSCFLRIRADGVVDCAR GQSAHSLLEIKAVALRTVAIKGVHSVRYLCMGADGKMQGLLQYSEEDCAF EEEIRPDGYNVYRSEKHRLPVSLSSAKQRQLYKNRGFLPLSHFLPMLPMV PEEPEDLRGHLESDMFSSPLETDSMDPFGLVTGLEAVRSPSFEK
N1-16	M-----DSSPLLQ--WGDPIRLRHLYTSGPHGLSSCFLRIRADGVVDCAR GQSAHSLLEIKAVALRTVAIKGVHSVRYLCMGADGKMQGLLQYSEEDCAF EEEIRPDGYNVYRSEKHRLPVSLSSAKQRQLYKNRGFLPLSHFLPMLPMV PEEPEDLRGHLESDMFSSPLETDSMDPFGLVTGLEAVRSPSFEK

Amino acids that differ from wild type FGF19 are shown in red. Red dash indicates deletion.

SUPPLEMENTARY DATA

Supplementary Table S5. Sequence of FGF19 Mutants in the C-terminal Region.

Name	Sequence
FGF19	RPLAFSDAGPHVHYGWGDPIRLRHLYTSGPHGLSSCFLRIRADGVVDCAR GQSAHSLLEIKAVALRTVAIKGVHSVRYLCMGADGKMQGLLQYSEEDCAF EEEIRPDGYNVYRSEKHRLPVSLSSAKQRQLYKNRGFLPLSHFLPMLPMV PEEPEDLRGHLESDMFSSPLETDSMDPFGLVTGLEAVRSPSFEK
C1	RPLAFSDAGPHVHYGWGDPIRLRHLYTSGPHGLSSCFLRIRADGVVDCAR GQSAHSLLEIKAVALRTVAIKGVHSVRYLCMGADGKMQGLLQYSEEDCAF EEEIRPDGYNVYRSEKHRLPVSLSSAKQRQLYKNRGFLPLSHFLPMLPMV PEEPEDLRGHLESDMFSSPLETDSMDPFGLVTGL----------
C2	RPLAFSDAGPHVHYGWGDPIRLRHLYTSGPHGLSSCFLRIRADGVVDCAR GQSAHSLLEIKAVALRTVAIKGVHSVRYLCMGADGKMQGLLQYSEEDCAF EEEIRPDGYNVYRSEKHRLPVSLSSAKQRQLYKNRGFLPLSHFLPMLPMV PEEPEDLRGHLESDMFSSPLETDS----------
C3	RPLAFSDAGPHVHYGWGDPIRLRHLYTSGPHGLSSCFLRIRADGVVDCAR GQSAHSLLEIKAVALRTVAIKGVHSVRYLCMGADGKMQGLLQYSEEDCAF EEEIRPDGYNVYRSEKHRLPVSLSSAKQRQLYKNRGFLPLSHFLPMLPMV PEEPEDLRGHLESD----------
C4	RPLAFSDAGPHVHYGWGDPIRLRHLYTSGPHGLSSCFLRIRADGVVDCAR GQSAHSLLEIKAVALRTVAIKGVHSVRYLCMGADGKMQGLLQYSEEDCAF EEEIRPDGYNVYRSEKHRLPVSLSSAKQRQLYKNRGFLPLSHFLPMLPMV PEE----------
C5	RPLAFSDAGPHVHYGWGDPIRLRHLYTSGPHGLSSCFLRIRADGVVDCAR GQSAHSLLEIKAVALRTVAIKGVHSVRYLCMGADGKMQGLLQYSEEDCAF EEEIRPDGYNVYRSEKHRLPVSLSSAKQRQLYKNRGFLPLSHFL------ ----------

Amino acids that differ from wild type FGF19 are shown in red. Red dash indicates deletion.

SUPPLEMENTARY DATA

Supplementary Table S6. Treatment Emergent Adverse Events in a Double-Blind, Placebo-Controlled trial of NGM282 in Patients with Type 2 Diabetes

	Placebo (n=20)	NGM282 2 mg (n=21)	NGM282 5 mg (n=19)	NGM282 10 mg (n=20)
Adverse Events by Severity Grade, n (%)				
Grade 1	11 (55%)	16 (76%)	18 (95%)	17 (85%)
Grade 2	6 (30%)	7 (33%)	9 (47%)	10 (50%)
Grade 3	1 (5%)	1 (5%)	2 (10%)	0 (0%)
Grade 4	0 (0%)	0 (0%)	0 (0%)	0 (0%)
Most Common (>10%) Adverse Events, n (%)				
Diarrhea	3 (15%)	6 (29%)	9 (47%)	8 (40%)
Nausea	3 (15%)	5 (24%)	9 (47%)	9 (45%)
Injection site bruising	2 (10%)	4 (19%)	5 (26%)	3 (15%)
Injection site pruritus	0 (0%)	3 (14%)	5 (26%)	5 (25%)
Headache	6 (30%)	2 (10%)	2 (10%)	2 (10%)
Injection site erythema	0 (0%)	0 (0%)	3 (16%)	6 (30%)
Frequent bowel movements	0 (0%)	2 (10%)	2 (10%)	3 (15%)
Vomiting	0 (0%)	1 (5%)	3 (16%)	1 (5%)
Abdominal distension	0 (0%)	1 (5%)	0 (0%)	3 (15%)
Serious Adverse Events, n (%)				
At least one serious adverse event	0 (0%)	0 (0%)	0 (0%)	0 (0%)